Journal of Solid State Chemistry **165,** 289–296 (2002)
doi:10.1006/jssc.2002.9529, available online at http://www.idealibrary.com on IDEAL®

Molecular Dynamics Studies of the Kinetics of Phase Changes in Clusters II: Crystal Nucleation from Molten $(RbCl)_{256}$ and $(RbCl)_{500}$ Clusters

Meihua Ma,* Wenqing Lu,† and Jinfan Huang‡,[1]

*Department of Chemistry, Nanjing Xiaozhuang College, People's Republic of China; †Department of Chemistry, Nanjing Normal University, People's Republic of China; and ‡Department of Chemistry, University of Michigan, Ann Arbor, Michigan, 48109

Received October 22, 2001; in revised form January 22, 2002; accepted February 1, 2002; published online March 27, 2002

Molecular dynamics computer simulations have been carried out to study the effects of cluster size and temperature on the nucleation rate of rubidium chloride clusters in the temperature range of 500–650 K. Clusters with 256 and 500 RbCl molecules have been studied and the results are compared with those obtained from 108 molecule clusters. The melting point (MP) of the clusters was observed to increase with the size of the clusters and can be described by a linear equation $MP = 997–405\ N^{-1/3}$, where *N* is the number of molecules in the cluster. The nucleation rate is found to decrease with increasing cluster size or increasing nucleation temperature. Both classical nucleation theory and diffuse interface theory are used to interpret our observed results.

Key Words: **rubidium chloride; crystal nucleation rate; interfacial free energy; size dependence; temperature dependence.**

1. INTRODUCTION

The main focus of our current research is the nucleation kinetics of phase transitions in condensed matter from electron diffraction (ED) experiments and/or computational experiments. In ED experiments, the clusters generated from supersonic jet expansions are probed with electron beams to monitor the phase transitions (1–7). In computational experiments, molecular dynamics simulations (MD) are performed based on the clusters (8–13). The differences between our ED approach and MD approach are the cluster size and the nucleation temperature. MD simulations were usually performed on smaller clusters and at lower nucleation temperature due to the limitations of the computer power. To compare the results from the two different approaches and to extrapolate the conclusion to the bulk materials, it is necessary to study the effect of cluster size and nucleation temperature on the nucleation rate.

[1]To whom correspondence should be addressed. Fax: + 1-734-647-4865. E-mail: jinfanh@umich.edu.

Alkali halides are among the simplest ionic materials. Crystalline alkali halides are widely used as optical materials. Therefore, the study of nucleation and crystallization on this type of materials has been an attractive topic both for science and technology. The nucleation of freezing of alkali halides with cluster diameter from 3 to 5 μm in high-temperature cloud chamber was performed by Buckle *et al.* (14). MD studies on $(NaCl)_{108}$ reported in our previous papers (11, 12) allow us to investigate the nucleation of freezing of $(NaCl)_{108}$ in the temperature range of 400–580 K. Our previous study on $(RbCl)_{108}$ (13) provided us with the nucleation rate and interfacial free energy information of this material in the temperature range of 500K–600 K. It is difficult to observe the crystallization of $(RbCl)_{108}$ at the temperature above 600 K in a reasonable simulation time period. To study the size effect and the temperature dependence of the nucleation, we performed MD studies on larger rubidium chloride clusters and at higher temperatures. In this paper, we report our MD results on $(RbCl)_{256}$ and $(RbCl)_{500}$ clusters in the temperature range of 550–650 K.

2. COMPUTATIONAL PROCEDURE

The MD simulations were performed in a similar way and the same interaction potential function used for $(RbCl)_{108}$ (13). Equal numbers of Rb^+ and Cl^- ions were initially arranged in a cubic-shaped box with each edge length of 4 and 5 times the unit cell which result in $(RbCl)_{256}$ and $(RbCl)_{500}$. The simulations for both clusters were started with 5000 time steps in a bath of 298.15 K and followed by another 5000 time steps at constant energy, then repeated 5000 time steps in a bath at 298.15 K and 10,000 time steps at constant energy. A series of heating stages then began at 320 K, each succeeding stage is 20° warmer than the previous one. Every stage was first simulated at constant temperature for 5000 time steps and then by 5000 time steps at

0022-4596/02 $35.00

constant energy. Heating was continued to 1080 K, which is ~ 90 K above the melting point of the bulk. Freezing simulation started from 1060 K and 1080 K for $(RbCl)_{256}$ and $(RbCl)_{500}$, respectively, each succeeding stage is 20° cooler than the previous one until the temperature reached 320 K. In all the simulations, the time step was set to 8 fs. Such a process corresponds to a heating/cooling rate of 2.5×10^{11} K/s.

The molten clusters for the nucleation study were first generated from the heating process mentioned above. After the $(RbCl)_{256}$ cluster was melted from the melting process at 1060 K, it was directly heated in a bath of 1060 K for 5000 time steps and followed by another 5000 time steps at the constant energy simulation. The heating was continued at 1060 K to form 16 clusters each with 2000 more timesteps than the previous one that gave 16 melted systems with different thermal histories for crystal nucleation studies. 16 melted systems of $(RbCl)_{500}$ cluster with different thermal histories were generated in a similar way but at a higher temperature(1080 K). There is no potential nuclei left for the crystal nucleation in all the molten systems generated in this way based on the diagnosis described in our previous paper (11).

Nucleation rates were investigated by immediately quenching the melted clusters into a heat bath at the temperatures of interest. The first temperature was chosen at 550 K, which is the middle temperature we used to crystallize $(RbCl)_{108}$ (13). $(RbCl)_{256}$ and $(RbCl)_{500}$ clusters are readily frozen into polycrystalline solid below this temperature. The highest temperature was chosen at 650 K, above this limit it is difficult to observe crystallization within a reasonable length of simulation time even for $(RbCl)_{500}$ cluster. Two other temperatures, 600 and 630 K, were chosen between the two limits.

The diagnostic tests, the estimation of nucleation rate and interfacial free energy followed the same methods used for $(RbCl)_{108}$. The details were given in our previous papers (11–13).

3. RESULTS

3.1. Melting

The selected images generated from the MACSPIN program for heating and cooling processes of $(RbCl)_{256}$ and $(RbCl)_{500}$ clusters are shown in Fig. 1.

Figure 2 presents the potential energy of clusters as a function of temperature. It is obvious that there is no unique temperature corresponding to the transition due to the extremely high heating rate and the large temperature increment between two successive heating runs. We select the midpoint of a jump on the potential energy curve that occurs when the cluster is being heated. The uncertainty is estimated from the two temperatures around the midpoint of the jump. According to this definition, the melting

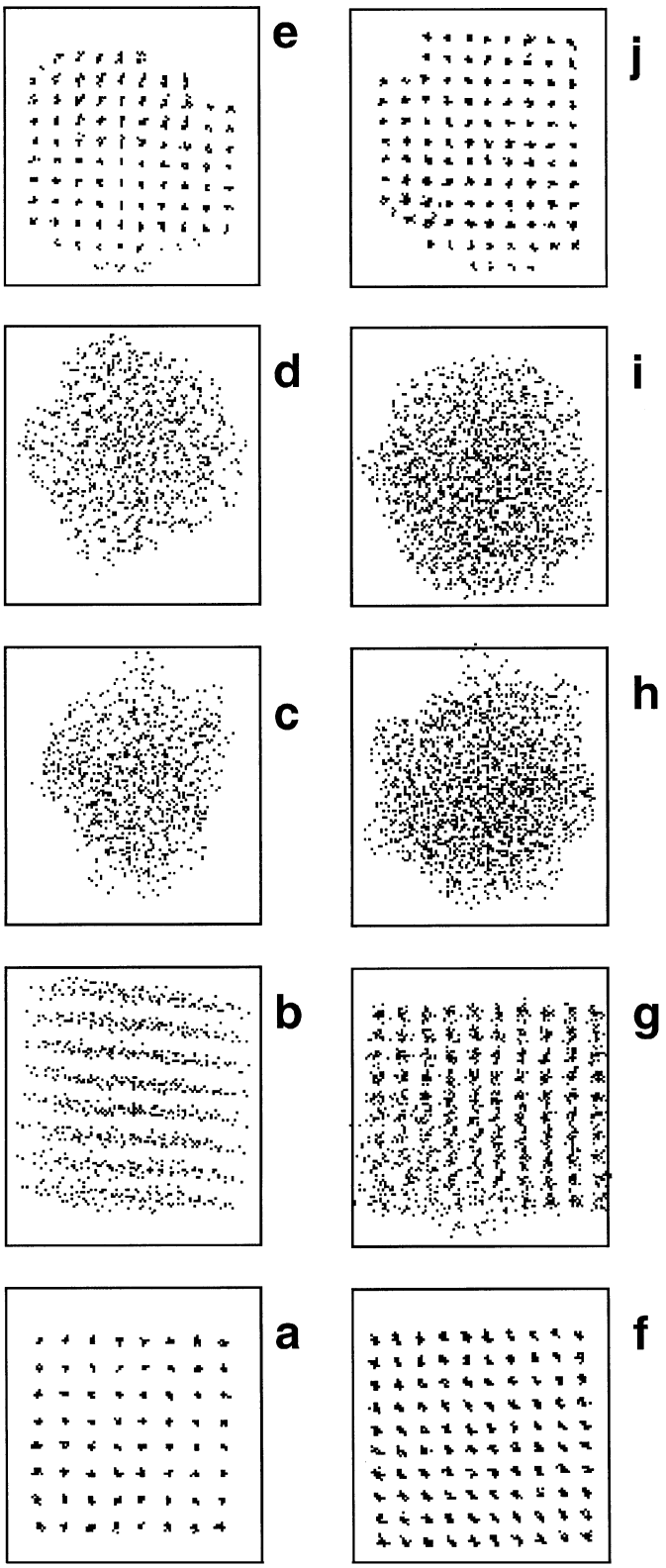

FIG. 1. Images of clusters at various stages of heating and cooling. Left-hand figures are for $(RbCl)_{256}$ at (a) 320 K, (b) 920 K, (c) 940 K, (d) 660 K (cooling), and (e) 320 K (cooling). Right-hand figures are for $(RbCl)_{500}$ at (f) 320 K, (g) 960 K, h. 980 K, (i) 700 K (cooling), and (j) 320 K (cooling).

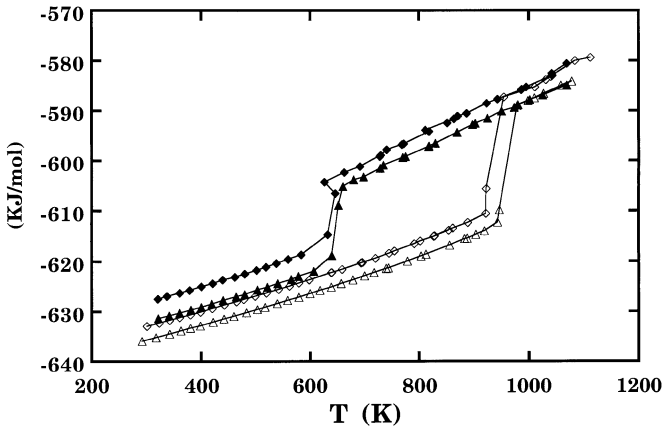

FIG. 2. Potential energy per mole of cluster as a function of temperature during the heating and the cooling stages. Empty triangle represents $(RbCl)_{500}$ during the heating process. Solid triangle represents $(RbCl)_{500}$ during the cooling process. Empty square represents $(RbCl)_{256}$ during the heating process. Solid square represents $(RbCl)_{256}$ during the cooling process.

temperatures and associated uncertainties are 960(16) and 937(16) K for $(RbCl)_{500}$ and $(RbCl)_{256}$, respectively, under the heating rate mentioned in the previous section. The melting temperature we reported for $(RbCl)_{108}$ is 880 K (13).

Apparently, the melting temperature increases with increasing cluster size. In Fig. 3, we plot the melting point of the cluster as a function of $N^{-1/3}$, where N is the number of RbCl molecules in a cluster. A linear curve fitting of simulated results along with the bulk melting point gives

$$T = 997 - 405\ \mathrm{N}^{-1/3}. \qquad [1]$$

The estimated bulk melting point is higher than the observed value; however, a rough relationship between the melting temperature and the cluster size can be seen from Eq. [1].

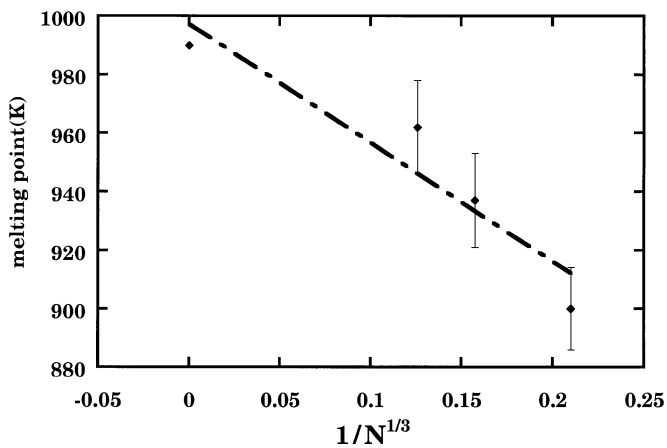

FIG. 3. Size dependence of the melting temperature of RbCl clusters. N is the number of molecules in a cluster.

Calvo and Labastic have studied the melting process for sodium fluoride [15] clusters with 6, 7, and 13 NaF molecules and found that the melting process appears to be a multistage phenomenon. However, the melting process for all the clusters we studied here reveals a one-step process. It seems that the cluster size makes a big difference here. We also noticed that the starting configuration is important to avoid getting the cluster into possible metastable configurations during the heating process.

A common characteristic for the molten RbCl clusters is that they are non-spherical, especially for the smaller clusters. The reasons for this have been given in a recent publication (16).

3.2. Freezing

The caloric curves for the cooling process of two clusters are also given in Fig. 2. We follow the same definition for the melting point to estimate the freezing temperature. The estimated values and the deviations are 625(20) and 645(15) K for $(RbCl)_{256}$ and $(RbCl)_{500}$, respectively, under the cooling rate of 2.5×10^{11} K/s. The stochastic nature of the nucleation initiating a phase change makes the freezing temperature unpredictable and unreproducible, we only use these temperatures as a reference to set the temperature range for nucleation studies. We found that if we quench the molten clusters into a bath with temperatures around the freezing temperature, we can see that the liquid crystallizes into single crystals within a reasonable simulation time. If the bath temperature is much lower than the freezing temperature, polycrystalline crystals are the main products, however, it is difficult to crystallize the liquid within a reasonable simulation time if the bath temperature is much higher than the freezing temperature.

As it is shown in Fig. 1 both $(RbCl)_{256}$ and $(RbCl)_{500}$ clusters froze into single crystals when they are cooled at the rate of 2.5×10^{11} K/s.

Crystallization of clusters was also observed when all the completely melted clusters were quenched into the bath temperature we selected. Most of the clusters froze into single crystals at higher bath temperature, however, most of the clusters froze into polycrystals at lower bath temperature. Table 1 lists the number of crystal domains formed in each cluster when they were quenched into the low-temperature bath.

The selected cluster images generated from the MACSPIN program for quenching a completely melted $(RbCl)_{500}$ cluster into a heat bath of 650 K are given in Fig. 4. A brief picture of the nucleation and crystal growth process in a $(RbCl)_{500}$ cluster during the quenching can be seen from this figure. The fluctuation of nucleation can be seen from Fig. 4a–c. The potential nuclei for the nucleation form and disappear in different places of the cluster (Fig. 4a and 4b), at the snap shot of the time after the cluster is kept

TABLE 1
Number of Critical Nuclei Formed

Cluster No.	550 K		600 K		630 K		650 K
	$(RbCl)_{256}$	$(RbCl)_{500}$	$(RbCl)_{256}$	$(RbCl)_{500}$	$(RbCl)_{256}$	$(RbCl)_{500}$	$(RbCl)_{256}$
1	2	3	1	2	1	2	2
2	3	2	1	1	1	2	1
3	1	2	1	2	1	1	2
4	3	2	1	2	1	2	2
5	1	2	2	1	2	2	3
6	1	3	2	1	1	1	1
7	1	3	1	4	1	1	1
8	2	1	1	3	1	1	1
9	1	4	1	3	1	1	1
10	1	2	1	2	1	1	2
11	1	3	1	1	2	2	1
12	2	2	1	1	2	2	2
13	1	3	3	1	1	2	1
14	1	4	2	1	1	1	1
15	1	4	1	2	1	1	1
16	2	3	2	2	1	1	1

in the bath of 650 K for $\sim$88,800 fs (Fig. 4c), all the potential nuclei for the nucleation disappeared. Once the critical nucleus is formed (Fig. 4d), the crystal starts to grow (Fig. 4e–4h). New nucleus can form and disappear (Fig. 4f and 4g) during the crystal growth. If the second nucleus becomes another critical nucleus a polycrystal will form.

3.3. Nucleation of Crystallization

Figures 5 and 6 plot the $\ln[N_n(t_n)/N_o]$ vs time t_n obtained from 48 quenching runs for $(RbCl)_{256}$, and 64 quenching runs for $(RbCl)_{500}$ at different temperatures, where N_0 is the number of total nucleation events studied, t_n is the time at which nth nucleation event N_n has taken place.

Based on the assumption that takes the total volume of a cluster as the effective volume V_e and all the clusters form single crystals, the calculated nucleation rates are listed in Table 2. Uncertainties are standard deviations based solely on the counting statistics (17)

$$\sigma_\tau/\tau = 1.10\ (N_0 - 3)^{1/2}, \qquad [2]$$

where τ is the measured property, σ_τ is the uncertainty of τ, and N_0 is the number of the events that the measurement was based on. It is obvious that the nucleation rate decreases with increasing the cluster size or increasing nucleation temperature. If more critical nuclei formed in a cluster, the nucleation rate has to be divided by a factor that equals the number of critical nuclei formed in the cluster. As it is shown in Table 1, at same temperature the chance to form polycrystals in larger clusters is higher than in smaller clusters. The size effect of the nucleation rate will be further confirmed if this factor is taken into account.

4. DISCUSSION

4.1. Size Dependence of Nucleation Rate

For a homogenous nucleation, the rate can be expressed by (18, 19)

$$J(T) = A\ \exp(-\Delta G^*/k_B T), \qquad [3]$$

where k_B is the Boltzman constant, T is the temperature, and ΔG^* is the free energy barrier to the formation of a critical nucleus of the new phase from the old phase.

From the classical nucleation theory (hereafter CNT), for a spherical nucleus in the freezing process ΔG^* is

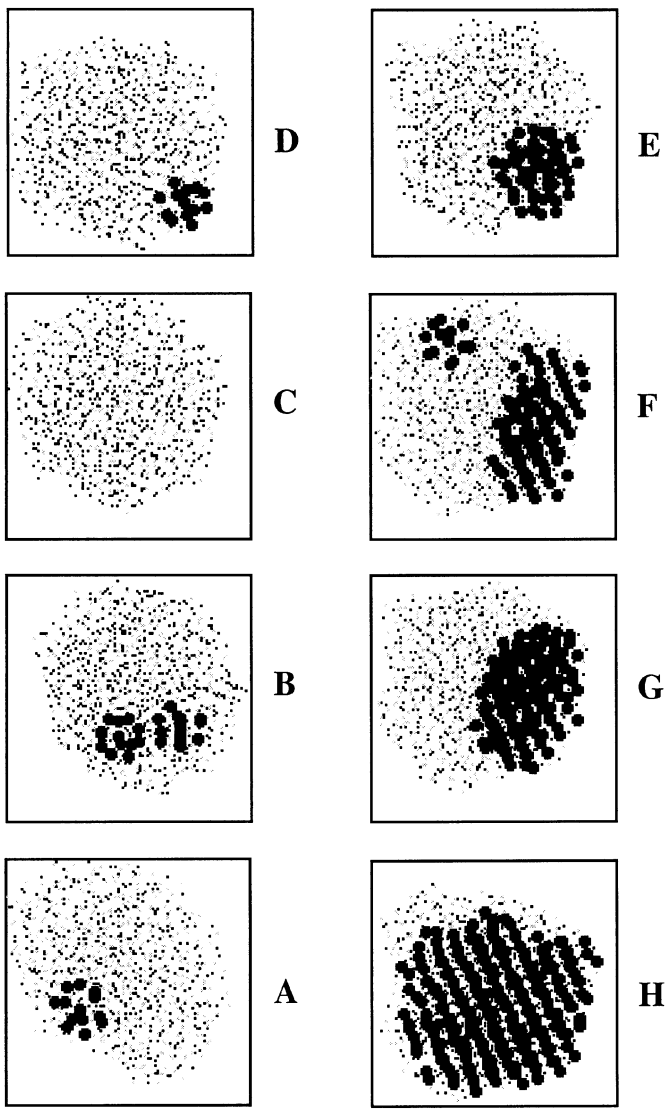

FIG. 4. Evolution of the critical nucleus and crystallization from $(RbCl)_{500}$ at 650 K. Heavy dark spots represent the chlorine ions that satisfy the "fcc unit:" (a) 800 fs; (b) 16 ps; (c) 88.8 ps; (d) 96.8 ps; (e) 104.8 ps; (f) 120.8 ps; (g) 128.9 ps; (h) 160.8 ps.

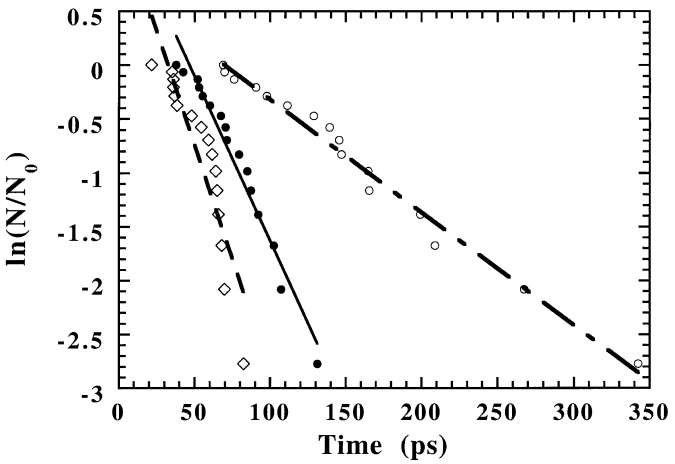

FIG. 5. $\ln[N_n(t)/N_0] \sim t$ plot from 48 MD runs on $(RbCl)_{256}$. Empty circle originates from 630 K. Filled circle originates from 600 K. Empty rhombus originates from 550 K.

given by

$$\Delta G^* = 16\pi\sigma_{sl}^3/[3(\Delta G_v + w')^2], \qquad [4]$$

in which σ_{sl} is the interfacial free energy between the solid and the liquid, ΔG_v represents the free energy change of freezing per unit volume, and w' the work per unit volume of changing the surface area of liquid phase during the formation of the nucleus which is expressed as

$$w' = P_L(\rho_l - \rho_s)/\rho_l, \qquad [5]$$

where P_L is the Laplace pressure $2\sigma_l/r_0$ inside the cluster, ρ's are densities of liquid and solid.

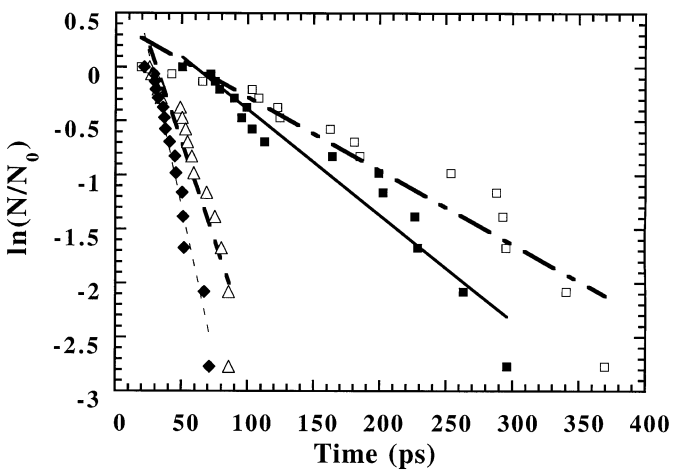

FIG. 6. $\ln[N_n(t)/N_0] \sim t$ plot from 64 MD runs on $(RbCl)_{500}$. Empty square originates from 650 K. Filled square originates from 630 K. Empty triangle originates from 600 K. Filled rhombus originates from 550 K.

TABLE 2
Calculated Nucleation Rate (m^{-3}/s^1)

Cluster	550 K	600 K	630 K	650 K
$(RbCl)_{108}$[a]	$3.6(1.0)\times10^{36}$	$7.3(2.2)\times10^{35}$		
$(RbCl)_{256}$	$1.7(0.5)\times10^{36}$	$6.8(2.0)\times10^{35}$	$2.5(0.8)\times10^{35}$	
$(RbCl)_{500}$	$1.2(0.4)\times10^{36}$	$5.7(1.7)\times10^{35}$	$2.0(0.6)\times10^{35}$	$1.4(0.4)\times10^{35}$

[a]From our previous result [Ref. (13)].

The free energy change of freezing per unit volume, $\Delta G_v(T)$ in Eq. [4] can be estimated from the standard thermodynamics

$$\Delta G_v(T) = (1/V)\int_{T_m}^{T} \Delta S_{fus}(T)\,dT, \qquad [6]$$

where V is the molar volume, $\Delta S_{fus}(T)$ is the molar entropy change of fusion at temperature T.

In the diffuse -interface theory (DIT) (20–23) ΔG^* is given by

$$\Delta G^* = -4\pi\delta^3\Delta G_v\psi/3, \qquad [7]$$

where δ is the thickness of the diffuse interface, and ψ can be defined as (17)

$$\psi = [2(1+Q)H^{-2} - (3+2Q)H^{-1} + 1]/\eta \qquad [8]$$

with $\eta = \Delta G_{fus}/\Delta H_{fus}$, $H = \eta\ (1+\zeta)$ with $\zeta = w'/\Delta G_v$, and $Q = (1-H)^{1/2}$.

The conventional formula for CNTs prefactor used is

$$A_{cl} = 16(3/4\pi)^{1/3}(\sigma_{sl}/k_BT)^{1/2}D/v_m^{2/3}\Delta r^2, \qquad [9]$$

where D is the coefficient of diffusion in the liquid, v_m is the volume of a molecule in solid, and Δr is the molecular jumper distance from the liquid to the solid usually taken to be $v_m^{1/3}$.

From the viewpoint of nucleation theory expressed in Eqs. [3]–[9], the dependence of nucleation rate on cluster size was mainly caused by the size dependence of property parameters going to these equations.

From the exponential part of Eq. [3], it is clear that any increase in ΔG^* will lower the nucleation rate. In CNT, the ΔG^* (Eq. [4]) is determined by the interfacial free energy between the liquid and the solid, σ_{sl}, the work, w', which is related to the volume change and the Laplace pressure, and the free energy change of freezing per unit volume, $\Delta G_v(T)$. σ_{sl} is supposed to change with temperature only but not with cluster size. It is obvious from Eqs. [4] and [5] that the w' term will make the smaller clusters have higher nucleation rate due to the larger Laplace pressure for smaller clusters.

Theoretically, $\Delta S_{fus}(T)$ in Eq. [6] can be calculated by the difference between the heat capacities of liquid and solid, ΔC_p. At a certain temperature, any increase in ΔC_p will make the $\Delta G_v(T)$ more negative. It is obvious from Eq. [4] that lowering the $\Delta G_v(T)$ will make the ΔG^* larger and result in a lower nucleation rate. Unfortunately, we lack ΔC_p information at the temperature of nucleation. In our previous research, we used the extrapolated liquid C_p either from the experimental data for bulk (11) or from the MD simulation for clusters (24). It is difficult to take the cluster size into account when we extrapolate C_p from the data for the bulk liquid. Furthermore, the temperature difference between the nucleation temperature we are studying and the temperature that the experimental data were obtained at is huge, for instance, the nucleation temperature range we studied for NaCl is 400–630 K, while the available bulk liquid C_p data are in the temperature range of 1073–1300 K. The extrapolation in such a huge temperature range might be very difficult to reveal the real world. In our previous research on KI, we derived C_p values for small liquid and solid clusters by using the caloric curves from heating and cooling processes in MD simulations (24). The information from this process gives the size effect on the heat capacity of small particles. We found that ΔC_p decreases with increasing cluster sizes. However, this process corresponds to negligence of the second term on the right-hand side of following equation:

$$C_p = \left(\frac{\partial E}{\partial T}\right)_p + p\left(\frac{\partial V}{\partial T}\right)_p. \qquad [10]$$

It is clear from Eq. [10] that the second term is highly related to the Laplace pressure.

Among the parameters going to the CNT prefactor that are given in Eq. [9], v_m, the volume of a molecule in the liquid, will be affected by the Laplace pressure. Smaller clusters usually have smaller v_m value and will make the prefactor larger. However, if the molecular jumper distance from the liquid to the solid taken to be $v_m^{1/3}$ is a correct assumption then it should be considered that there is no effect from v_m. This left the diffusion coefficient, D, as the only consideration for size effect in the prefactor part. As we reported in our previous paper, smaller clusters usually have larger diffusion coefficient due to the higher percentage of surface molecules (24). The larger diffusion coefficient will result in a higher nucleation rate.

The DIT essentially uses a similar prefactor as CNT does. In the exponential part of Eq. [3], w' plays a similar role to affect the nucleation rate. However, the $\Delta G_v(T)$ affects the nucleation rate in DIT in the opposite way as it does in CNT. We may neglect the influence on the size effect from the $\Delta G_v(T)$ if both theories work fine in the current system.

TABLE 3
Interfacial Free Energy and Diffuse Interface Thickness[a]

	CNT	DIT
T/cluster	σ_{sl} (A_{CNT})	δ
500 K		
$(RbCl)_{108}$[b]	0.0390	1.95
550 K (average)	0.0423	1.86
$(RbCl)_{108}$[b]	0.0415	1.88
$(RbCl)_{256}$	0.0425	1.87
$(RbCl)_{500}$	0.0430	1.83
600 K (average)	0.0465	1.92
$(RbCl)_{108}$[b]	0.0480	2.01
$(RbCl)_{256}$	0.0460	1.86
$(RbCl)_{500}$	0.0455	1.79
630 K (average)	0.0478	1.84
$(RbCl)_{256}$	0.0485	1.87
$(RbCl)_{500}$	0.0470	1.80
650 K		
$(RbCl)_{500}$	0.0485	1.76

[a]The unit for σ_{sl} is in J/m^2, and δ is in Å.
[b]From our previous result [Ref. (13)].

Figure 4d gives an example of the position of one critical nucleus. From all of our observations, all the critical nuclei are formed around the surface of molten clusters. Smaller clusters have higher ratio of surface molecules, which is another explanation of why the nucleation rate is higher in smaller clusters at the same nucleation temperature.

From the above analysis it seems the higher nucleation rate in smaller clusters is mainly related to the high surface area ratio, higher surface tension, and higher diffusion coefficient of the smaller clusters.

4.2. Interfacial Free Energy and the Diffuse Interface Thickness

All the properties going to Eqs. [3]–[9] to derive the interfacial free energy between the solid and the liquid are listed in Table A1 of Ref. (13).

The temperature dependence of the interfacial free energy from CNT presented in Table 3 was fitted into a widely used equation

$$\sigma_{sl}(T) = \sigma_{sl}(T_1)(T/T_1)^n, \qquad [11]$$

where an n value of 0.83 for RbCl in the temperature ranges from 550 to 650 K was obtained from our nucleation rate. Nucleation data for the freezing of mercury give an n value of $\sim$ 0.3–0.4 (25). It is interesting to note that the n value for RbCl is much larger than the values for other systems.

The diffuse interface thickness δ parameter derived from DIT with our nucleation rates seems to increase with decreasing temperature though the value at 600 K is out of the

trend due to a very high value from $(RbCl)_{108}$. The observed trend is consistent with our observations from KI (26). The temperature dependence can be approximately described by an equation similar to Eq. [11] with the m value of 0.2

$$\delta(T) = \delta(T_1)(T_1/T)^m. \quad [12]$$

According to Granasy (20), the δ value can be used to estimate the structure factor k_t. The relationship between the δ and the structure factor k_t is

$$k_t = \delta v_m^{-1/3}, \quad [13]$$

where v_m is the volume of a molecule. It leads to a k_t value of 0.37 from Eq. [12] if we use the v_m value of $5.79 \times 10^{-29}\,m^{-3}$ for a molecule in the liquid and the δ value of 1.70 Å at the melting point. For a series of metalloids the k_t value was found to be ~ 0.32 (27), while for metals the value of 0.45 was used (27). The k_t value of 0.37 for RbCl surprisingly fits into that value range.

The well-known Turnbull empirical equation relating the heat of fusion at the melting point and interfacial free energy through the structure factor is (27)

$$\sigma_{sl} = k_t \Delta H_{fus}/(V^2 N_A)^{1/3}, \quad [14]$$

where N_A is Avogadro's constant, V is the molar volume (whether of solid or liquid was not specified). We calculated the interfacial free energy at melting point by adopting 0.37 for the structure factor and the heat of fusion at melting point (18,409 J/mol). At the melting point of the bulk, the calculated value of 53.9 mJ/m^2 from Eq. [14] is lower than the value of 68.7 mJ/m^2 from Eq. [11].

One available experimental interfacial free energy data for rubidium chloride was reported by Buckle and Ubbelohde at a temperature of 827 K (14). Interestingly, the value of 59.2 mJ/m^2 estimated from Eq. [11] at 827 K is not very far from their reported experimental value of 55.7 mJ/m^2 at this temperature.

4.3. Size of Critical Nuclei

As it is shown in Fig. 4, the number of molecules in crystallized phase sharply increases when the crystal starts to grow. The information about the critical nuclei may be derived from the snapshot of the system at the time not very far before the time that the crystal starts to grow. After viewing hundreds of images of the clusters around the time that crystal starts to grow, we found a subcluster with all molecules in it satisfing our criteria formed shortly before the crystal starts to grow, as displayed in Fig. 4d. Its size is a function of temperature. The average sizes of such clusters are around 33, 40, 55, and 70 RbCl molecules at temperatures of 550, 600, 630, and 650 K, respectively.

From the CNT the size of the critical nuclei can be calculated from

$$n^* = (32/3)\pi V^2 N_A[\sigma_{sl}/(\Delta G_{fus} - Vw')]^3, \quad [15]$$

where ΔG_{fus} and V represent the molar free energy of fusion and molar volume, and N_A is Avogadro's number. The calculated sizes of critical nuclei from Eq. [15] are 6, 9, 13, and 15 at 550, 600, 630, and 650 K.

In DIT the size of the critical nuclei can be calculated from

$$n^* = 8\pi\delta^3\psi/(3V_m) \quad [16]$$

where δ is the diffuse interface thickness, V_m represents the volume of a molecule, and ψ was given in Eq. [8]. The calculated sizes of critical nuclei from DIT are 4, 7, 9, and 11 at 550, 600, 630, and 650 K.

The difference between the number counted from our simulation and the number calculated from nucleation theories is approximately the number of surface molecules of the critical nucleus from the counting. If the number from nucleation theories is more meaningful, then surface molecules that form the Turnbull-ordered liquid layer surrounding the critical nucleus may be a good assumption. On the other hand, if the number from our counting is more meaningful, then we can describe the critical nucleus as consisting of an ordered core and a disordered solid layer at the interface that is part of the critical nucleus

5. CONCLUDING REMARKS

The size and temperature effects on the nucleation rate of crystallization from molten rubidium chloride have been studied in the temperature range of 550–650 K by MD simulations. The nucleation rate was found to decrease with increasing cluster size or temperature. Laplace pressure plays a major role for the size effect on the nucleation rate.

Both CNT and DIT were used to interpret the nucleation rates obtained from this report. It was found that the temperature dependence of interfacial free energy obtained from this report could reasonably reproduce the interfacial free energy value obtained from the experiment. The sizes of the critical nuclei calculated from CNT and the interfacial free energy obtained from the present study are in good agreement with those counted from the cluster images similar to those in Fig. 4 if the surface molecules of the critical nuclei from the counting method are neglected.

All the results described here are based on the Born–Mayer–Huggins potential. Further studies with modified potential functions which will include the dispersion and polarization interactions are being carried out. New results will be reported in a forthcoming paper.

ACKNOWLEDGMENTS

This work was supported by a grant from Nanjing Normal University of P. R. China and a grant from the National Science Foundation of USA to the University of Michigan.

REFERENCES

1. L. S. Bartell and T. S. Dibble, *J. Phys. Chem.* **95,** 1159 (1991).
2. T. S. Dibble and L. S. Bartell, *J. Phys. Chem.* **96,** 2317 (1992).
3. J. Huang and L. S. Bartell, *J. Phys. Chem.* **98,** 4543 (1994).
4. J. Huang and L. S. Bartell, *J. Phys. Chem.* **99,** 3924 (1995).
5. J. Huang, W. Lu, and L. S. Bartell, *J. Phys. Chem.* **99,** 11,147 (1995).
6. J. Huang, W. Lu, and L. S. Bartell, *J. Phys. Chem.* **100,** 14,276 (1996).
7. T. S. Dibble and L. S. Bartell, *J. Phys. Chem.* **96,** 8603 (1992).
8. J. Chen and L. S. Bartell, *J. Phys. Chem.* **97,** 10,645 (1993).
9. S. Xu and L. S. Bartell, *J. Phys. Chem.* **99,** 10,446 (1995).
10. K. Kinney, S. Xu, and L. S. Bartell, *J. Phys. Chem.* **97,** 13,550 (1996).
11. J. Huang, X. Zhu, and L. S. Bartell, *J. Phys. Chem. A* **102,** 2708 (1998).
12. L. S. Bartell and J. Huang, *J. Phys. Chem. A* **102,** 8722 (1998).
13. H. Deng and J. Huang, *J. Solid State Chem.* **159,** 10 (2001)
14. E. R. Buckle and A. R. Ubbelohde *Proc. Roy. Soc. London. Ser. A* **259,** 325 (1960); E. R. Buckle and A. R. Ubbelohde *Proc. Roy. Soc. London. Ser. A* **261,** 189 (1961); E. R. Buckle and A. R. Ubbelohde *Proc. Roy. Soc. London. Ser. A* **261,** 197 (1961).
15. F. Calvo and P. Labastie, *J. Phys. Chem. B* **102,** 2051 (1998).
16. L. S. Bartell, *J. Mol. Struct.* **445,** 59 (1998); L. S. Bartell, *Surf. Sci.* **397,** 217 (1998).
17. Y. Chushak, P. SantiKary, and L. S. Bartell, *J. Phys. Chem. A* **103,** 5636 (1999).
18. D. Turnbull and J. C. Fisher, *J. Chem. Phys.* **17,** 71 (1949).
19. E. R. Buckle, *Proc. Roy. Soc London. Ser. A* **261,** 189 (1961); E. R. Buckle, *Proc. Roy. Soc London. Ser. A* **261,** 197 (1961).
20. L. Granasy, *Mater. Sci. Eng. A* **178,** 121 (1994).
21. L. Granasy, *Europhys. Lett.* **24,** 121 (1993).
22. L. Granasy, *J. Non-Cryst. Sol.* **162,** 301 (1993).
23. L. Granasy, *J. Phys. Chem.* **99,** 14,183 (1995).
24. J. Huang and L. S. Bartell, *J. Mol. Struct.* **567,** 145 (2001).
25. D. Turnbull, *J. Chem. Phys.* **20,** 411 (1952).
26. J. Huang and L. S. Bartell, *J. Phys. Chem.*, accepted for publication.
27. D. Turnbull, *J. Appl. Phys.* **21,** 1022 (1950).